The Engineering Resource For Advancing Mobility

400 COMMONWEALTH DRIVE WARRENDALE, PA 15096

SAE Technical Paper Series

821469

Flight at Supernormal Attitudes

Thomas H. Strom and William J. Alford, Jr.
Dynamic Engineering Inc.
Newport News, VA

Aerospace Congress & Exposition
Anaheim, California
October 25-28, 1982

ISSN 0148-7191

821469

Flight at Supernormal Attitudes

Thomas H. Strom and William J. Alford, Jr.
Dynamic Engineering Inc.
Newport News, VA

ABSTRACT

In Supernormal Flight (SNF), the aircraft's wing is either partially or completely stalled, while the longitudinal stabilizing and control surfaces are deflected to approximately the same magnitude, but of opposite sign, as the aircraft's angle of attack so that they remain effective through large ranges (approaching 90°) of angles of attack, pitch, and flight path. Some potential advantages of SNF include: improved safety through prevention of spins; rapid recovery from undesirable stalls and spins; steep descents and approaches to landings; precise, steep, survivable recoveries of remotely piloted vehicles (RPVs); and enhanced maneuverability and agility. Free-flight, wind tunnel, and analytic results are presented on example aircraft models to illustrate and substantiate the proposed applications and advantages.

THE PURPOSES OF THIS PAPER ARE TO:

- Define Supernormal Flight (SNF).
- Describe some potential performance enhancements due to SNF.
- Present model flight, wind tunnel, and analytic results for example general aviation and fighter aircraft using SNF.
- Identify concerns and additional data needs.
- Recommend actions required for full-scale application of SNF.

SUPERNORMAL FLIGHT

Until about 1978, the region beyond stall was considered an unacceptable flight regime frequently characterized by uncontrollable flight in spins and the undesirable "deep stall". This condition is characterized by a stable, high angle of attack trim point from which recovery may be difficult or impossible. NASA, in Reference 1, defines deep stall as an "....out of control condition at α greater than stall with no significant motions other than high rate of descent".

Because it is now possible, through use of an all-moving horizontal tail on aft-tailed configurations or large span, large chord elevons on tailless configurations (References 2 and 3), to provide stable and controllable flight at extremely high attitudes, and since motions other than high rates of descent can be commanded and sustained with sufficient thrust levels, examination and redefinition of the safety and usefullness of the extremely high attitude flight regions was assessed to be required.

Supernormal Flight (SNF) is concerned with flight at extraordinary angles of attack, the resulting substantial changes in the pitch and flight path angles, and the attainment of flight path and vertical velocities which are not otherwise available to the pilot.

An illustration that defines the important SNF parameters and the Dynamic Engineering, Inc. (DEI) all-moving horizontal tail control concept for SNF is presented in Figure 1.

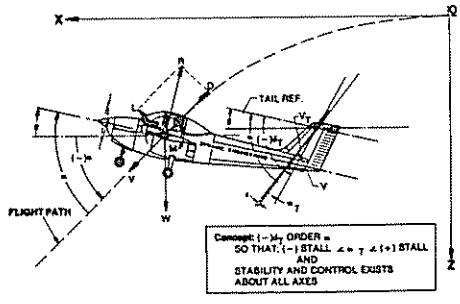

Fig. 1 - Definitions and Concept Illustration

Definitions and symbols utilized in this and other figures are presented in Appendix A.

0148-7191/82/1025-1469$02.50

In the illustration of Figure 1, a general aviation aircraft is shown descending in a trimmed condition along a steep flight path angle at a very high angle of attack but with only a modest pitch attitude. The thrust vector is representative of full power conditions; the aerodynamic forces are to scale relative to the weight vector.

As shown in Figure 1, the essence of the DEI longitudinal control concept (References 2 and 3) is to deflect the tail, or large chord elevons, to magnitudes of approximately the same order, but of opposite direction, as the airplane angle of attack so that the effective tail aerodynamic angle of attack is below the tail stall angle and is thus capable of providing both stability and control. The longitudinal control concept can be generally described as an active application of the passive Goldberg "Dethermalizer" concept (Reference 4), which is used to safely recover free flight glider and airplane models when they become involved in flyaway conditions. As will be shown subsequently, stability and control about the lateral and directional axes is also maintained.

In most cases, the upper limit of normal flight and the lower limit of SNF are associated with conditions for maximum lift, beyond which the wing is completely stalled. For some aircraft configurations, however, (e.g., those employing wings with high leading edge sweep angles or incorporating strakes) partial flow separations of the wing or control surfaces may induce stability problems below the attitudes for maximum lift and impose premature limits to the normal flight regions. Solutions of these problems will allow flight above these premature limits. Flight above these limits is also considered of a supernormal nature.

The upper limits of SNF cannot as yet be adequately specified since the variety of configurations tested at very high angles of attack (approaching 90°), and for which appropriate detailed force, moment, and pressure data is available, are severly limited. On configurations for which adequate data is available (some of which are presented herein) it appears that upper limits of angles of attack (and pitch) can approach 70° to 90°, with flight path angles ranging from large positive values to large, near vertical, negative, or descent values depending on the available and commanded thrust levels. The corresponding forward and vertical velocities can also have wide variations ranging from zero to much higher-than-normal values depending on the angle of attack and thrust levels.

POTENTIAL PERFORMANCE ENHANCEMENTS

Some of the potential applications associated with SNF are described in the following introductory illustrations. Subsequent discussions present and describe qualitative movie records and quantitative wind tunnel and analytic results to substantiate these proposed applications.

Stall survivability enhancement is illustrated in Figure 2, (Reference 23) which

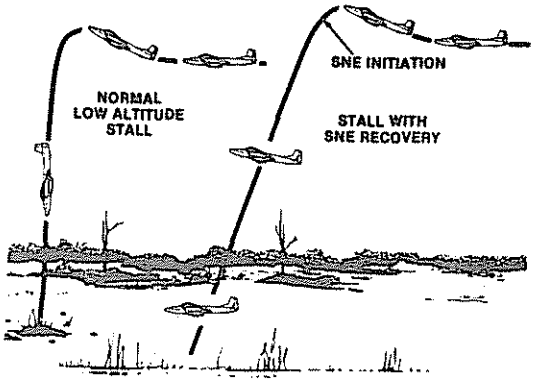

Fig. 2 - Stall Survivability is Enhanced through Attitude Control (SNE)

compares the steep, nose-down attitudes normally associated with low-altitude, usually fatal, stalls with the essentially level pitch attitudes that can be commanded and sustained through large deflections of the all-moving, supernormal tail or elevator (SNE). With no power, the descent rate would still be high, but the attitude is in the direction to be survivable. With sufficient power on, the descent rates could be considerably decreased and recovery attempted if sufficient altitude were available. In addition, it may be possible to utilize supplementary wing-trapped vortex concepts such as described in References 5 through 8 to provide lift to reduce the vertical velocities still further.

Spin recovery is illustrated in Figure 3, (Reference 23),

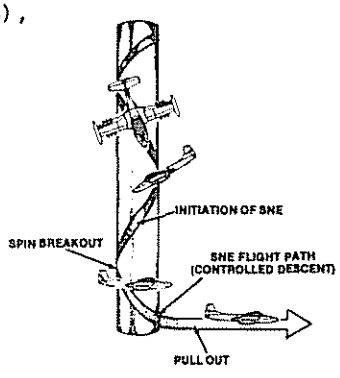

Fig. 3 - Spin Recovery Facilitated with All-Moving Tail Control

which shows that shortly after SNE initiation, the aircraft stops spinning and a level flight pull-out is effected by rapidly returning the tail position to its normal range. NASA (Reference 9) has recently demonstrated this application of SNE controls as effective in spin recoveries of both lightly-loaded general

aviation aircraft models with normal spin characteristics, and heavily-loaded fighter aircraft models that normally have flat, fast spinning characteristics that make recovery very difficult with use of conventional control techniques.

Precise survivable recovery of RPVs is described in Figure 4 (Reference 23).

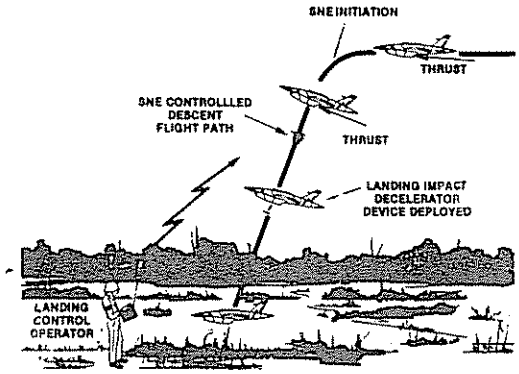

Fig. 4 - Precision Recovery of RPVs

In this sequence, the Landing Control Operator initiates a SNF descent by deflecting the control and modulating thrust to establish the desired descent flight path. It is envisioned that a landing impact decelerator could be deployed to absorb the landing energy.

It is suggested that fuel usage reductions may be attained by future V/STOL aircraft in the landing mode by executing low thrust level SNF approaches. Such an application by a V/STOL type aircraft is illustrated in Figure 5 (Reference 23).

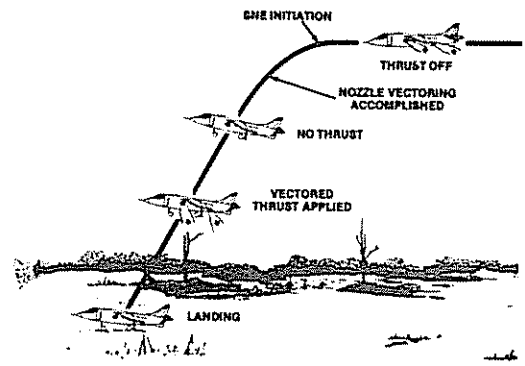

Fig. 5 - Fuel Saving Descent Utilizing SNF

At the end of the steep approach vectored thrust is applied to effect a low vertical velocity landing.

An example of SNF application to future STOL aircraft is illustrated in Figure 6, (Reference 23),

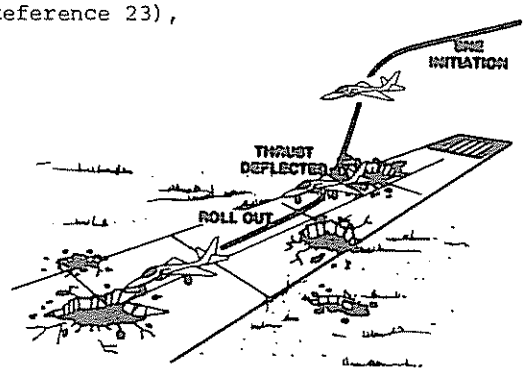

Fig. 6 - Application of SNF to Future STOL Aircraft

which depicts an aircraft making a steep descent to a damaged runway and deflecting its thrust to modulate sink rate. It may also be possible to utilize supplementary wing trapped vortex concepts, discussed earlier to reduce both forward and vertical velocities, and to provide reduced ground-roll distances.

Additional tactical maneuvering capabilities are described in Reference 10 through use of a combination of advanced technologies in the form of electronic digital control, the aerodynamic advancements of delta wings and "Supermaneuverability". Supermaneuverability is defined as "...combined post-stall (PST) and direct force (DFM) capability. PST represents the ability of the aircraft to perform controlled tactical maneuvers beyond maximum lift angle of attack up to at least 70°; DFM represents the ability of the aircraft to yaw and pitch independently of the flight path or to maneuver at constant fuselage attitude." It was concluded in Reference 10 that a fighter concept employing these technologies would feature, combined in one design, excellent supersonic performance thus improving the use of future medium-range missiles (MRMS), a conventionally unachievable level of short-range air combat capabilities, and an extremely short field performance.

In summary, SNF as proposed here means safe and useful flight at angles of attack much greater than normally associated with maximum lift (e.g., α = 30° to 90°). The ranges of unaccelerated trim and control of pitch and flight path angle, and the associated flight path and vertical velocities, can be greatly expanded. In addition, the dynamic and accelerated maneuvering turn rates, agility, aiming and pointing characteristics can be significantly enhanced.

FREE-FLIGHT MODEL TEST RESULTS

Motion picture records of the flights of a number of scaled radio controlled, free-flight models of both generic and specific general aviation, aerobatic, remotely piloted

surveilance vehicles (RPVs) have been obtained by Dynamic Engineering Incorporated during the last eight to ten years; these are summarized in Reference 11. The results of these motion picture records are largely qualitative in as much as the models did not employ on board, physical data measuring systems, nor were adequate background distance or altitude reference scales available. For the oral version of the paper, the movie records largely speak for themselves. For the written version, the results are described in an approximate, qualitative manner assisted by a limited number of photographs reproduced from the films for each of the models. The interested reader is invited to visit DEI facilities to view the film records or have the authors visit in order to present and describe the motion picture results.

PILOTING TECHNIQUE DEVELOPMENT - The first test sequence utilized a propeller-driven model of a typical general aviation airplane of about 1/8 scale. This model employed a straight wing with a span of about 1.3m (4.4 ft.) and an aspect ratio of 5.8. The aft-mounted, all-moving horizontal tail was mounted below the wing chord plane and was capable of deflections of up to -90° (T.E. up).

The flight test range was located near a coastal region of the Chesapeake Bay having an abundant foliage of tall, dense marsh grass which allowed safe, non-destructive recoveries of the model during the learning and piloting technique development phase.

A pre-flight photo of the model horizontal tail in the deflected position is presented in Figure 7(a). After launch the model was flown to initial altitudes of about 50 meters (150-160 ft.) and positioned for entry into a SNF steep descent. SNF entry was executed by rapidly commanding a horizontal tail deflection of -60° or greater; a stable, steep, high rate of descent was established by reducing power to idle.

The model was piloted to various headings by use of the rudder since the ailerons were not very effective. Directional and lateral stability and control were available, and appeared to be improved by deflection of the horizontal tail to large, trailing edge up positions. This improved effectiveness is presumed due to unstalling the horizontal tail which blanks the rudder and vertical tail at its lower deflections (Reference 12).

After a series of practice SNF entries, piloting exercises, and recoveries, the model was forced to spin by the pilot (Figures 7(b) and 7(c)). Subsequent to establishing a stable spin of several turns, rapid recovery was effected by application of the SNF tail deflection (Figure 7(d)). The model stopped spinning in about 1/2 to 3/4 of a turn. A return to normal flight could be effected by simply reducing the tail to cruise position and increasing power to the desired level. The

(a) - Preflight illustration of all-moving horizontal tail deflection. $\delta_h = -70°$

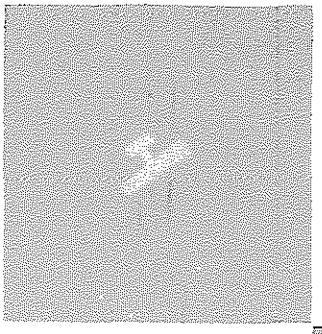

(b) - Model entering into spin.

(c) - Model in spin after several turns.

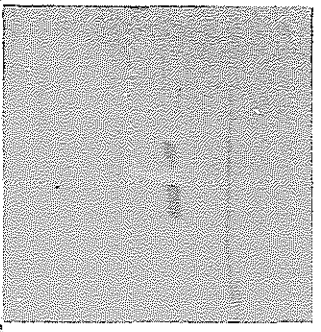

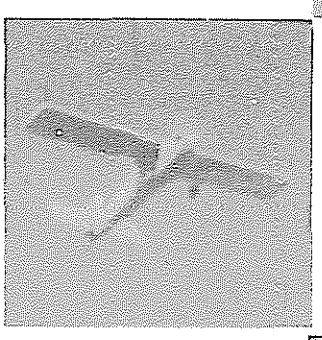

(d) - Horizontal tail deflected to effect spin recovery

(e) - Model in steep descent to landing after spin recovery

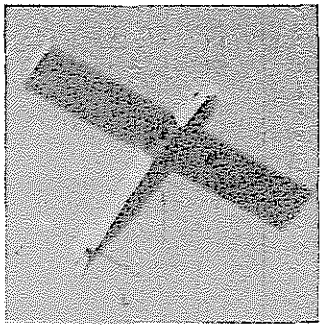

Figure 7 - Selected frames of 1/8 scale General Aviation model before and during SNF.

model could also be made to continue descent in SNF as shown in Figure 7(e).

The second test series employed a 1/6-scale powered model of the Bellanca "CITABRIA" aerobatic airplane. Illustrative views of this model entering into and during SNF descents to landing are shown in Figure 8. This airplane model also employed a high straight wing with a span of 1.75m (5.75 ft.) and an aspect ratio of 6.4. The all-moving horizontal tail was mounted below the wing chord plane.

As illustrated in Figure 8, considerable piloting technique experience was gained by executing a number of power-off and -on SNF entries, turns, and descents, and the model's handling qualities were investigated over a wide range of pitch attitude and flight path angles by variations in thrust level. The take-off and landing site used in this series of tests was a packed dirt strip used for conventional model aircraft flights. In all cases, successful recoveries were made, as illustrated in Figure 8(e), even with relatively high flight path angles (up to $\gamma = -70°$) and descent rates.

CONCEPT VERIFICATION AND DEMONSTRATION - These phases of the model test programs employed both tailless flying wing (Figures 9 and 10) and aft-tailed configurations (Figure 11).

The flying wing model had a leading edge sweep of about $\lambda = 20°$ and an aspect ratio of 4.9. The engine and propeller were located above the wing chord plane on the vertical tail (Figure 9(c)). The model utilized differentially deflectable large-chord, full-span elevons for both pitch and roll-control. These elevons could be deflected up to $\delta_e = -90°$ (T.E. up) for SNF. Although no wind tunnel data were obtained for this specific model, wind tunnel force and moment data, and free flight model records on a conceptually similar model of the Chance Vought XF7U-1 model (sweep angle of 35° and an aspect ratio of 3, Reference 13), substantiated that stable and controllable flight could be accomplished to very high angles of attack.

A number of SNF experiments were made with the flying wing model, including hand launches followed by SNF descents to concrete runways and transitions from normal flight to SNF flight and returns to normal flight. Examples of these flights are illustrated in Figure 9. Repeatable, precise approaches were made with spot landings at the pilot's feet as shown in Figure 10. It should be noted that due to the location of the engine with its thrust above the model center line, no power-on descents were possible because the engine thrust offset would cause nose-down moments of sufficient magnitude to prohibit SNF.

The fourth series of the concept demonstration model flights was made with a series of three models of 1/2-scale RPVs that were designed and fabricated for use in proposals

(a) - Entry into SNF mode by deflection of all-moving horizontal tail

(b) - Model is stabilized, descent with idle power

(c) - Model in SNF descent

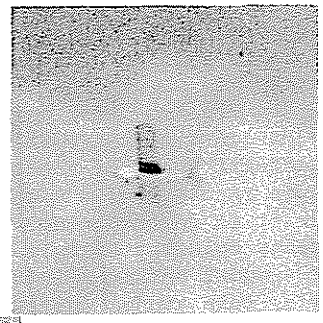

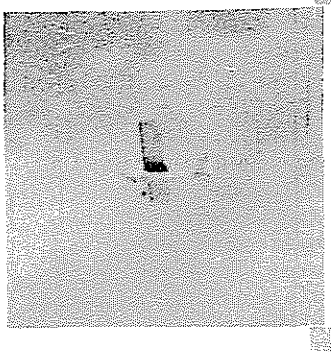

(d) - Pilot prepares model for landing

(e) - Power increased to increase pitch attitude and to decrease flight path angle and sink rate at landing

Figure 8 - Illustrative views of a 1/6-scale Citabria during entry into and during SNF descents

in response to the U.S. Army's "Little R" program. Photographs of these models are presented in Figure 11. The models employed different wing areas, aspect ratios, and wing-loadings to investigate these effects on handling and recovery characteristics. Three of the models are shown in Figure 11(a).

An idle-power descent of the model with a straight wing span of 1.5m (5 ft.) and an apsect ratio of 6 is shown in Figure 11(b). The movie records also provide views of the model making: (a) a series of four SNF descents with transitions to normal flight; (b) SNF descents with landing and taxi-back-to-pilot which demonstrates repeatable flight-ready condition; (c) normal approaches and landing for comparison of normal and SNF flight path and descent velocities; (d) two SNF approaches and landings taken from a distance and shown in slow motion (film speed 45% of normal speed) to demonstrate approach angles; and (e) several flights with the high-wing loading model showing descent-to-landings followed by taxi returns to verify repeatable results without damage to the model Some example views of some of these flights are shown in Figures 11(c) through 11(e).

MILITARY AIRCRAFT SPIN RECOVERY TESTS - The effectiveness of the all-moving tail surface on spin recovery of a high performance fighter aircraft is demonstrated in Figure 12, which presents selected example NASA photographs of an F-4 model during spin tests in the NASA Langley spin tunnel (Reference 9).

In figure 12(a), the model was launched so that it entered into its characteristic fast, flat spin. After several turns (Figure 12(b)), the all-moving tails were deflected to about -90° (T.E. up), as indicated in Figure 12(c), by the deployment of the control-activation identity target. The rate of spin rapidly decreased and recovery began, as depicted in Figure 12(d); the model completed recovery rapidly after only a few turns, as shown in Figure 12(e). The NASA movie records indicated that the SNF recovery technique was a considerable improvement over the normal technique which was to deflect the rudder 30° against the turn, the ailerons 30° with the turn, and the elevators +21° (T.E. down). Once again, this improved spin recovery characteristic with SNF is presumed due to unstalling the horizontal tail which improves the effectiveness of the vertical tail (Reference 12).

GENERAL AVIATION AIRCRAFT CHARACTERISTICS

WIND TUNNEL TEST RESULTS - In order to better understand the characteristics of aircraft operating in the SNF mode and to provide quantitative data to proceed to full-scale manned flight, a wind tunnel investigation was made utilizing a 1/4-scale flying model of a two-place, general aviation aircraft similar to the Piper PA-38 TOMAHAWK (Reference 14). A three-

(a) - Entry into SNF with idle power

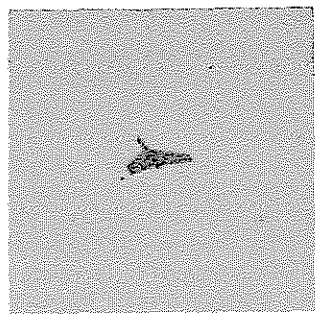

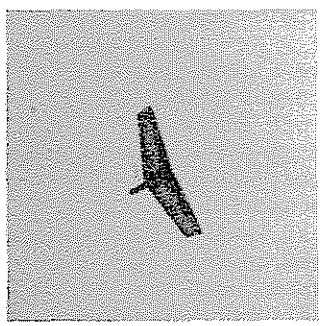

(b) - Stable and controllable steep descent

(c) - SNF landing approach

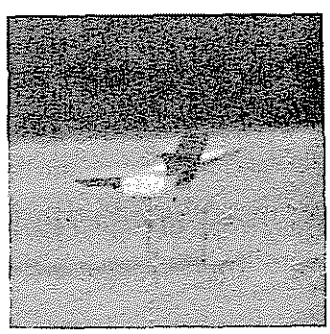

Figure 9 - Selected frames of flying wing model in SNF and descent

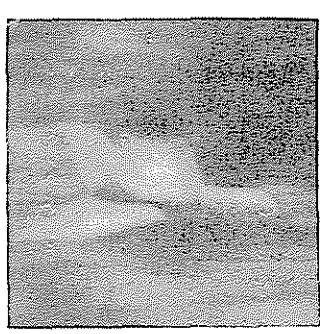

(a) - Precise landing approach

(b) - Repeatable spot landings at pilot's feet

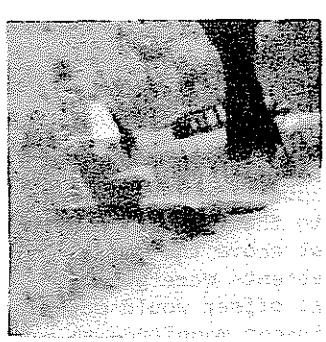

Figure 10 - Precision landing of flying wing model using SNF controls

(a) - Models being prepared for flight

(b) - SNF entry with idle power

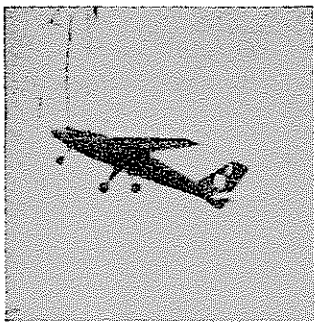

(c) - Stabilized and controlled descent with power modulated

(d) - Approach to landing

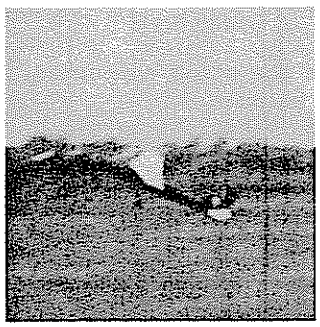

(e) - Landing touch-down with power applied to regulate descent velocity

Figure 11 - Views of 1/2-scale RPV models before and during SNF maneuvers and landings

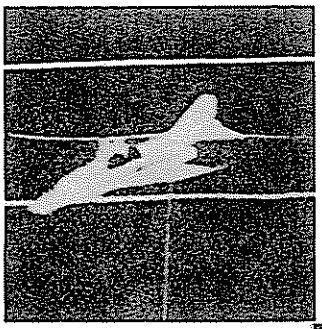

(a) - Model entering a fast flat spin

(b) - Model after several turns

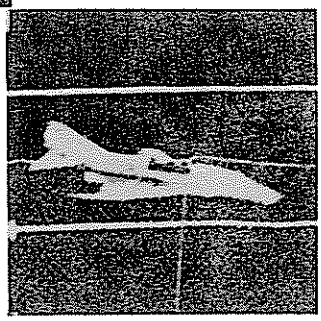

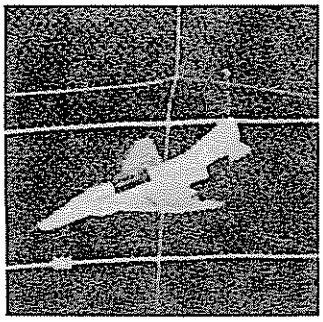

(c) - All-moving tails deflected to effect recovery

(d) - Spin slows

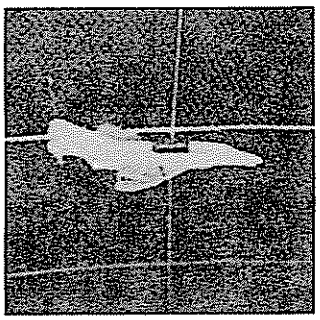

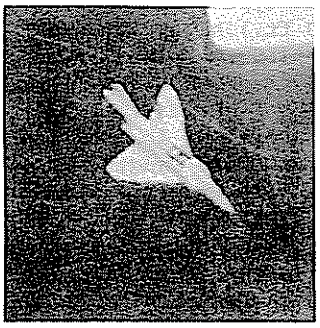

(e) - Model recovers

Figure 12 - NASA photographs of F-4 model equipped with SNF tails to improve recovery. Tests made in the Langley Spin Tunnel

view drawing of this model is presented in Figure 13. The tests were made with the control

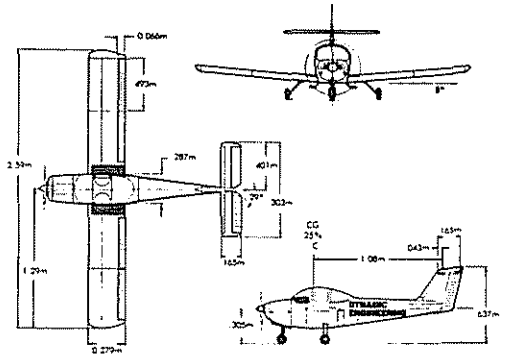

Fig. 13 - Three-View Drawing of a General Aviation Wind Tunnel Model

surfaces at a series of selected, fixed positions and without power.

The model had an overall length of 1.77m (5.8 ft.), a wing span of 2.59m (8.5 ft.), a constant chord of 0.286m (0.9375 ft.), a reference wing area of 0.740m^2 (7.97 sq. ft.), and an aspect ratio of 9.07. The cantilevered low wing employed a NASA GA(W)-1 airfoil section with a 17-percent-thickness-to-chord ratio and had 1° incidence at the wing root and a linear twist to provide -1° incidence at the wing tip. The horizontal tail had a span of 0.800m (2.625 ft.), a chord of 0.165m (0.542 ft.) and was mounted in a high position, relative to the wing, near the tip of the vertical tail. The aileron chord was .24C and spanned the outer 50 percent of the wing. The deflection limits were -26° T.E.U. and 14° T.E.D. The rudder extended the full length of the vertical tail; its deflection limits were $\pm$29°.

The model was tested in the NASA-Langley Research Center's 30- by 60-foot tunnel. This facility is a subsonic continuous flow, double return, open-throat type tunnel. The test section is 9.14m (30 ft.) high, 18.29m (60 ft.) wide, and 17.07m (56 ft.) long. The tests were conducted at a speed of about 17.68 mps (58 fps) which corresponds to a dynamic pressure of 191.52 n/m^2 (4 lb/ft^2) and a Reynolds number, based on chord length, of approximately 3.5 x 10^5.

Longitudinal and lateral force tests were conducted over an angle-of-attack range of 0° to 90° and a sideslip range of $\pm$10°. Control effectiveness was determined for tail deflections from 0° to -90° and for full right and left deflection of the ailerons and rudder.

The force and moment data were obtained by use of an externally mounted, sting supported, six-component strain gage balance. Because of the relative size of the model, no tunnel blockage or jet boundary corrections were applied to the data.

A photograph of the model in the Langley 30- by 60-foot wind tunnel is presented in Figure 14. Here the model is shown at an

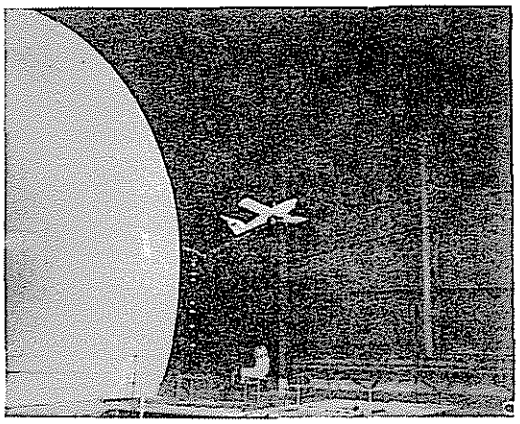

Fig. 14 - Photograph of the Model in the NASA-LaRC 30- by 60-Foot Tunnel α = 20° δ_h = -70°

angle of attack of about 20° and the tail is deflected to about -70°. The tunnel air return passage is on the left of the photograph. A photograph of the model at α = 90° and δ_h = -70° is presented in Figure 15. The

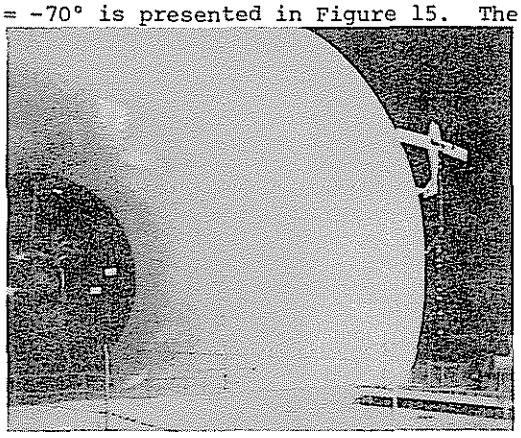

Fig. 15 - Photograph of the Model in the NASA-LaRC 30- by 60-Foot Tunnel α = 90° δ_h = -70°

model is shown attached to the sting supported, six-component strain gage balance.

A brief summary of the vehicle's aerodynamic characteristics are presented in Figures 16 through 21. Additional detailed data and analysis are contained in Reference 14.

LONGITUDINAL CHARACTERISTICS - The stability and control characteristics of the general aviation aircraft are presented in Figure 16 as the variation of pitching moment coefficient as a function of angle of attack for selected deflections of the all-moving horizontal tail. These data indicate that above α = 10°, the tail-off configuration was stable up to α = 90°. The horizontal tail

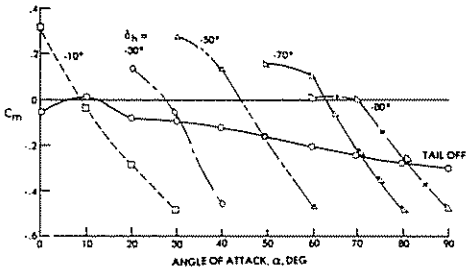

Fig. 16 - Pitching Moment Coefficient vs. Angle of Attack for Several Horizontal Tail Deflections and Tail-Off

was clearly capable of providing stability and control for angles of attack to at least 63° and most likely to about 70° for the reference moment center at 0.25C.

The trimmed lift, drag, and resultant force coefficients are presented in Figure 17.

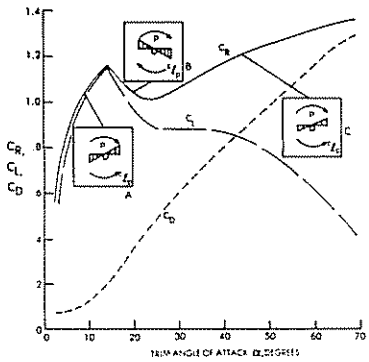

Fig. 17 - Longitudinal Force Characteristic Variation with Angle of Attack for the General Aviation Airplane Model

Maximum lift occurs at about $\alpha = 14°$ and has a value of about 1.18. This relatively low value is assessed to be associated with the low test Reynolds number of 3.5×10^5.

Data presented in References 15 and 16 on a low wing general aviation aircraft tested at Reynolds no. varying from about 2.9×10^5 to 3.5×10^6 indicated a large effect of Reynolds no. on the lift, normal force, and axial force coefficients from approximately 10° to 30°. Above $\alpha = 30°$ the effect of Reynolds no. was relatively small. Therefore, the wind tunnel data above $\alpha = 30°$ are assessed to be reasonably representative of conditions that will exist at full scale.

The variation of the resultant force coefficient with angle of attack is important and interesting from at least two points of view: (1) when its slope is positive (i.e., $\frac{\partial C_R}{\partial \alpha} > 0$) the configuration would be expected to possess positive damping in roll which assists in spin resistance and prevention, at least for aircraft whose wings employ low sweep (Reference 17), and (2) it is a prime parameter in governing the aircraft's trimmed velocity characteristics throughout the angle-of-attack range, particularly at low power settings (Reference 18). The insert figures show the distribution of incremental spanwise load due to rolling velocity p. In the region below stall ($\alpha < 14°$), the slope of the resultant force curve is positive. As the rolling velocity p increases, the downgoing wing increases its angle of attack (and hence lift) as shown in insert A. This situation leads to the development of a rolling moment due to rolling, C_{ℓ_p}, which is in a direction to oppose or slow the motion. This situation holds under conditions when the resultant force curve has a positive slope (increasing force with increasing angle of attack).

As the angle of attack progresses past stall (region B), we see that the downgoing wing panel, while increasing its angle of attack, suffers a loss in resultant force which gives rise to the distribution shown in B. Here the rolling moment due to roll is in the direction of the roll velocity, a propelling moment. This situation (Reference 17) has been related to a tendency to enter a spinning flight condition.

Region C is a region of positive slope of C_R vs. α, and while the slope is reduced, it still gives rise to a rolling moment which damps the motion. Region C, therefore, is a region in which there is no "tendency" to spinning, and controlled flight at high angles of attack is readily accomplished. In establishing SNF the stall (region A) is approached; as the model stalled, the angle of attack was rapidly changed from $\alpha = 14°$ to $\alpha = 25°$ to avoid spinning. Beyond $\alpha = 25°$, superflight is possible provided adequate control about the airplane axes is available.

The longitudinal trim, control, and flow field characteristics are presented in Figure 18. The figure shows that the vertical

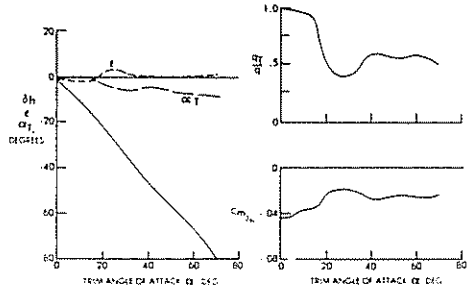

Fig. 18 - Longitudinal Control and Flow Field vs. Trim Angle of Attack for the General Aviation Airplane Model

velocity flow field angle ε changes from a small downwash to an upwash angle at about the stall angle of attack. The curve labeled α_t depicts the variation in tail angle of attack (to trim) as a function of airplane trimmed angle of attack. The value of α_t always remains less than 10° and therefore retains its ability to trim and control the aircraft up to the limit of the test data. The ability to keep the angle of attack of the horizontal tail low, irrespective of the airplane angle of attack is the key to controllable supernormal flight. The tail angle of attack is kept low by using the extraordinarily high tail deflection angles δ_h shown in the figure.

The dynamic pressure ratio at the tail q_t/q is also shown on the figure. For the configuration displayed (a straight wing, "T" tail airplane) the first depression in the q_t/q curve $\alpha \simeq 16°$ to 36° represents the effect of the passage of the stalled wing wake over the horizontal tail. At a trimmed angle of attack of about 40°, the value of q_t/q rises to a level in excess of 0.5. As a result of the fuselage wake on the tail, the value remains at about this level through the trimmed angle of attack range to about $\alpha = 70°$. The loss in dynamic pressure at the tail is due to low energy wakes shed from other parts of the airplane and flowing over the tail, resulting in a loss in the control effectiveness parameter, $C_{m_{\delta_h}}$. However the curve shows that $C_{m_{\delta_h}}$ retains substantial effectiveness throughout the trimmed angle of attack range and is responsible for the crisp control exhibited in the model flight tests shown to date.

LATERAL-DIRECTIONAL CHARACTERISTICS - The stability characteristics are presented in Figure 19; the control characteristics are presented in Figures 20 and 21. These data are presented with respect to the stability axes (Reference 19).

The directional stability parameter, C_{n_β}, Figure 19, was positive throughout the angle-of-attack range and actually increased significantly with increasing α. The effective dihedral parameter, C_{ℓ_β}, varied greatly with angle of attack but remained positive $(-C_{\ell_\beta})$ up until about α = 80°. The variation of the parameters C_{n_β} and C_{ℓ_β} thus described would indicate static stability throughout most of the angle of attack range.

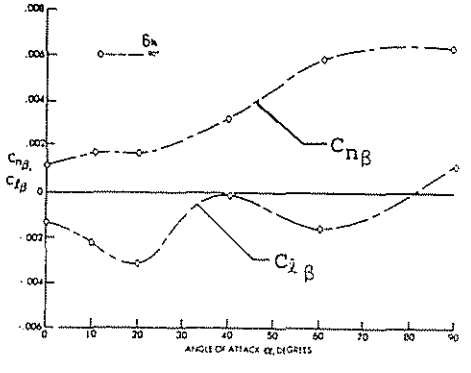

Fig. 19 - Variation of Lateral-Directional Stability Characteristics with Angle of Attack, $\delta_h = -90°$

The incremental rolling-moment coefficients associated with full right deflections of the ailerons, ΔC_{ℓ_a}, Figure 20, indicate that the rolling-moment available from the aileron decreased sharply above wing stall but retained some positive effectiveness to about α = 60°. The rolling-moment due to rudder control, ΔC_{ℓ_r}, changed from negative (adverse) to positive near wing stall, and remained of substantial magnitude throughout the angle-of-attack range thereby allowing control even though the ailerons become ineffective and even reversed in effectiveness. It should be noted that the rudder effectiveness is probably a function of power setting due to the slipstream effect on the fin.

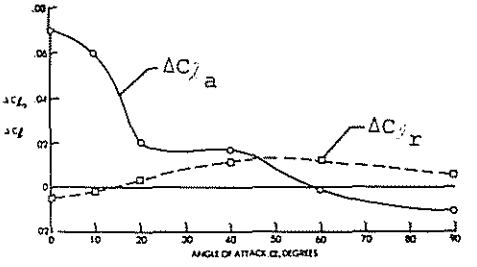

Fig. 20 - Incremental Rolling-Moment Coefficient Variation with Angle of Attack for Full Right Deflection of Aileron and Rudder

The rudder yawing moment increment, ΔC_{n_r}, Figure 21, is shown to decrease in a

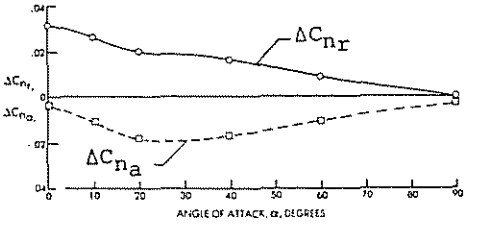

Fig. 21 - Incremental Yawing-Moment Coefficient with Angle of Attack for Full Right Deflection of Aileron and Rudder

near linear manner until it becomes zero at 90° angle of attack. The level of yawing moment generated by the ailerons, ΔC_{n_a}, varies in magnitude with increases in angle of attack but always remains adverse (i.e., opposite to the direction of roll).

In summary, the static lateral-directional data show that the configuration is stable and that there is control available for maneuvering. At angles of attack approaching 90°, these control moments are not of the magnitude or direction normally experienced in unstalled flight but could be used for orienting the airplane in the desired direction with a modified piloting technique.

ESTIMATED FULL-SCALE CHARACTERISTICS

Trimmed flight path characteristics of the all-moving tail configuration were calculated using the wind axes equations of motion (References 14 and 18). A full-scale airplane wing area of 11.61m^2 (125 ft^2), a weight of 689.5 kg (1520 lbs.), an initial altitude of 1.52 km (5000 ft.), and thrust-to-weight ratios of 0 to 0.25 were assumed. The aerodynamic data of Figure 17 were utilized without corrections for Reynolds number effects. As noted earlier, the results for angles of attack less than 30° will be pessimistic in as much as the full-scale aircraft lift would be higher and the drag less than for the model values. Above 30° the results are assessed to be reasonable. It should be noted that the calculations did not account for the aerodynamic effects of the slip-stream impinging on the airplane components.

The flight path and vertical velocities are presented in Figure 22 as variations with

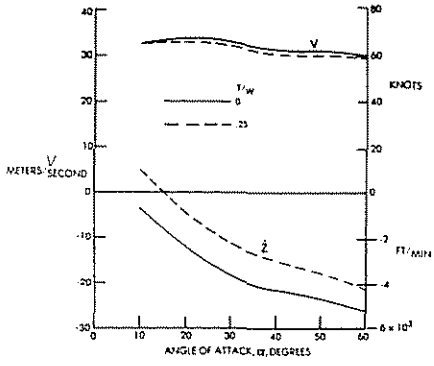

Fig. 22 - Variation of Flight Path and Vertical Velocities with Angle of Attack for Two Power Levels

angle of attack for the two power settings. The flight path velocity decreases only slightly with increases of either angle of attack or thrust-to-weight ratio. The vertical velocity increases negatively with increases in angle of attack due to decreases in the flight path angle, Figure 23, as drag

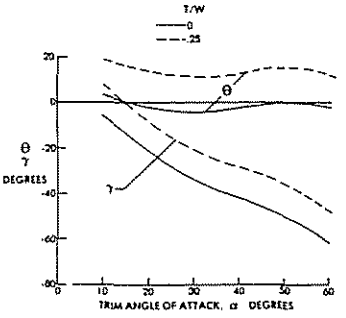

Fig. 23 - Variation of Attitude and Flight Path Angle with Angle of Attack for Two Power Levels

increases. The descent rate varies from about 9 m/s (1900 ft/min.) at α = 15° to about 26 m/s (5200 ft/min.) at α = 60° for a T/W = 0. Increasing T/W to 0.25 decreases the descent rate to 0 at α = 15° and to approximately 20 m/s (4300 ft/min.) at α = 60°.

For a T/W = 0, the flight path angle, Figure 23, varies from -15° at α = 15° to approximately -62° at α = 60°, and the pitch attitude correspondingly varies from 0° to -2°. Increasing T/W to 0.25 causes the flight path angle and the pitch attitude both to be increased by an essentially constant increment of about 14°.

In general, these calculated characteristics correlate qualitatively with flight results on a 1/6 scale model of a Tomahawk presented in Reference 20 and with the results of the free flight model tests presented earlier. It is also noted that the descent velocities at the higher angles of attack are much higher than could be safely tolerated at landing touchdown. For acceptable sink rates to be obtained, the aircraft would have to be derotated at sufficient altitude in its approach path, have additional energy absorbtion capability provided in the landing gear, or have the available power increased.

Therefore, the principle advantages of supernormal flight in respect to general aviation safety seem to lie in: (1) spin recovery as described earlier, and (2) stall recovery. Once past the stall angle of attack, the airplane attitude can be held near zero and recovery to normal flight can be undertaken safely. In the event that the stall happens at an altitude which is too low to effect a recovery prior to impact, the control principles described herein can be utilized to adjust the final flight path. In addition application of the control will assure that the impact attitude is in the range for best occupant survival. The assumption that survivable structure is in place between the occupant and the impact area may be tenuous

at this point in time, but with the impact attitude controlled, the designer will certainly find the job of providing deformable, safe, energy absorbing structure with which to protect the passengers and crew easier.

MODIFIED LIGHTWEIGHT FIGHTER CHARACTERISTICS

In order to determine potential applications and advantages of SNF to other classes of aircraft, studies were made (Reference 18 and 21) of both the trimmed and accelerated performance characteristics of an example, high-performance, lightweight fighter (LWF) aircraft configuration.

A line drawing of the assumed airplane is presented in Figure 24. This configuration

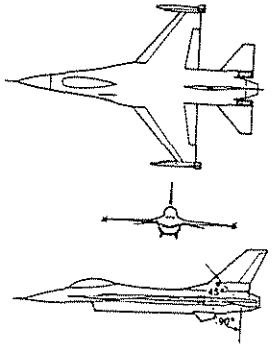

Fig. 24 - Sketch of the Lightweight Fighter Configuration used in the Study

is similar to an existing, high-performance lightweight fighter in the ten-ton weight class (F-16) with a maximum thrust-to-weight ratio (T/W) somewhat greater than unity. The longitudinal control system modification assumed for the present study to provide acceptable control to very high angles of attack consisted of the utilization of an all-moving horizontal tail of from approximately +45° (T.E. down) to -90° (T.E. up) with direct pilot access to the controls (i.e., no control surface or angle of attack limiters). For conditions of low velocity and dynamic pressure where aerodynamic controls are ineffective, it was assumed that the controls would be augmented by reaction controls or thrust vectoring. The aircraft weights and control systems complexities that would accompany these assumed changes have not been accounted for in this preliminary performance study.

The assumed LWF aerodynamic characteristics based on low speed wind tunnel tests; reported in Reference 22, are presented in Figure 25. To illustrate the potential of SNF applied to the assumed LWF aircraft, Figure 26 has been prepared, which presents the various flight regions on the angle of attack - Mach number domain. It should be pointed out that compressibility effects have been

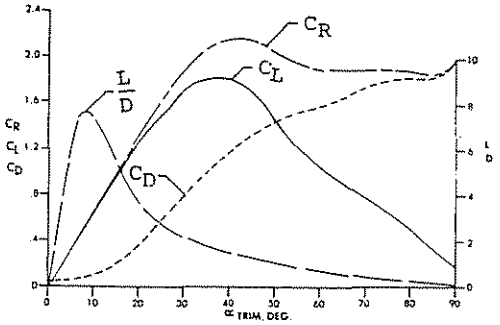

Fig. 25 - Longitudinal Force Characteristic Variation with Angle of Attack, Lightweight Fighter Model

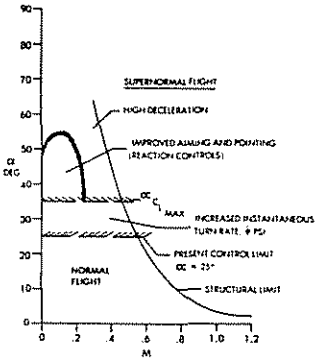

Fig. 26 - Supernormal and Normal Flight Regimes for a Lightweight Fighter

ignored in the preparation of the Figure. Neglecting, then, the small changes in angle of attack at constant lift due to compressibility, Figure 26 shows the region of normal flight below α = 25 and under the structural load limit line to the line of limit Mach number of the airplane.

SNF for the LWF, therefore, lies in the region above the normal control limited angle of attack line, α = 25°, even though the wing $C_{L_{max}}$ is not reached until α = 35° (see Figure 25). Above the normal trim angle, potential advantages in both trimmed and accelerated flight can be exploited.

In high angle of attack trimmed flight, SNF can provide a wide range of variations in flight path and vertical velocities and in pitch and flight path angles. In one extreme, with full power, it should literally be possible to stand the LWF on its tail in hover, while at the other extreme, with modulated power, it should be possible to attain very steep, rapid or slow descents and approaches to landings.

As shown in Figure 26, in accelerated flight SNF can provide: (1) increased instantaneous turn rate, (2) improved aiming and pointing, and (3) high deceleration.

TRIMMED UNACCELERATED CAPABILITIES

Two-degree-of-freedom equations along and normal to the flight path were employed (Reference 18) to calculate the trimmed and unaccelerated flight path and vertical velocities, and the flight path and pitch attitudes, for the angle of attack range extending from 30° to 90° and for thrust-to-weight ratios varying from 0 to 1.0. The wing loading assumed was 3.26 kn/m^2 (68 lb/ft^2), which corresponds approximately to half fuel loading; the initial altitude was 3.05 km (10k ft.).

The flight path velocity shown in Figure 27 varies in a somewhat elliptical manner,

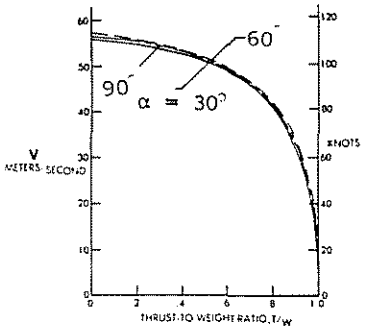

Fig. 27 - Variation of Flight Path Velocity with Thrust to Weight Ratio for Several Angles of Attack

with increases in the T/W having a maximum value somewhat greater than about 55 m/sec (107 knots) at T/W = 0 and decreasing to zero at T/W = 1.0. For the angles of attack shown, only minor differences are exhibited. As seen in Figure 28, somewhat lower velocities

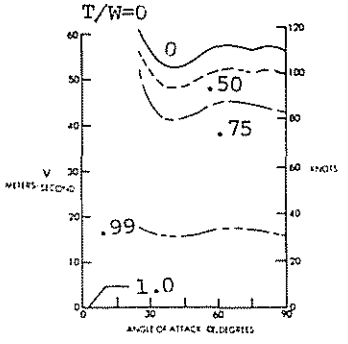

Fig. 28 - Variation of Flight Path Velocity with Angle of Attack for Several Thrust to Weight Levels

are in evidence in the region between α = 35° to α = 45°. These characteristics are traceable to the variations of the resultant force coefficient, C_R, presented in Figure 25, since the flight path velocity varies inversely with the square-root of the resultant force coefficient (Reference 18), particularly for the lower T/W's.

In general, the flight path angle variation with thrust-to-weight, Figure 29,

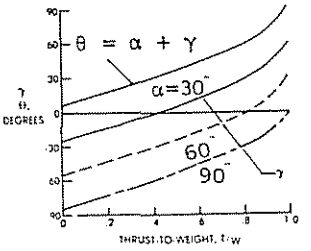

Fig. 29 - Variation of Flight Path and Pitch Attitude Angles with Thrust to Weight Ratios

is reasonably linear, with T/W up to values approaching 0.75 above which the slopes progressively increase to maximum values at T/W = 1.0. The curves for the various flight path angles are essentially displaced by the incremental differences between the chosen α's, in this case 30°. This is due to the pitch attitude, θ, being essentially constant with angle of attack for the various T/W's. The pitch attitude varies from about 5° at T/W = 0 to 90° at T/W = 1.0.

The characteristics of the flight path velocities (Figures 27 and 28) combine with the flight path angle characteristics, Figure 29, to provide the vertical velocity characteristics presented in Figure 30. The

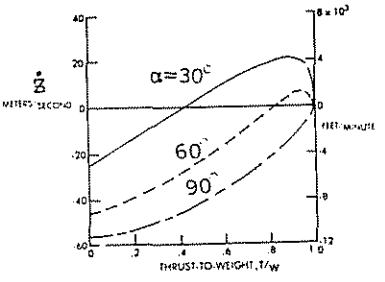

Fig. 30 - Variation of Vertical Velocity with Thrust to Weight Ratio at Several Angles of Attack

vertical velocity increases with increases in T/W to about 0.8 or greater, and then decrease rapidly to zero at T/W = 1.0 as a result of the flight path velocity tending to zero at T/W = 1.0. As an example, for α = 60°, the vertical velocity varies from about -45 m/s (-8858 ft/min.) at T/W = 0 to zero at T/W = 0.82, becomes about 8 m/s (1575 ft/min.) at T/W = .95, and goes to zero at T/W = 1.0.

To further illustrate the attitudes,

velocities and forces associated with trimmed unaccelerated SNF flight, the illustration of Figure 31 presents graphically these parameters

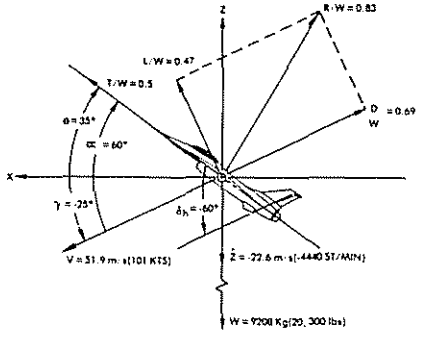

Fig. 31 - Graphic Illustration of Attitudes, Forces, and Flight Direction for SNF, $\alpha = 60°$ T/W = 0.50

for the case of $\alpha = 60°$ and T/W = 0.50. For this example, the pitch attitude assumes a value of 35° while the flight path is -25°, the velocity is approximately 52 m/s (100 kts); and the descent rate is -22.6 m/s (-4400 ft/min).

MANEUVERING AND AGILITY CONSIDERATIONS

INSTANTANEOUS TURN RATE - Increasing the turn rate allows the bending of the flight path toward or away from an adversary and is therefore judged to be a desirable design feature. Turn rate, $\dot{\Psi}$, as a function of Mach number, is presented in Figure 32 for a wing loading of 3.26 kn/m^2 (68 lb/ft^2) and an initial altitude of 3.05 km (10k ft). The calculations did not include the thrust component in the direction normal to the flight path and are therefore conservative in nature.

As indicated in Figure 32, increasing

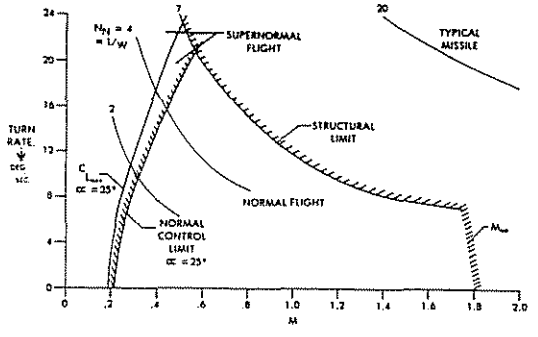

Fig. 32 - Turn Rate as a Function of Mach Number for Several Load Factors

load factor at a given Mach number increases turn rate. At a given load factor, the turn rate is inversely proportional to velocity and Mach number. The curve representing the structural limit load factor illustrates this trend. The low speed end of the diagram shows a "normal" control limit line which represents the turn rate at the lift coefficients attainable at $\alpha = 25°$ which is the condition where the existing unmodified LWF begins to experience longitudinal stability and control problems.

Turning performance could be improved if the tail control actuators were modified to allow trim to angles of attack above 25°. Increasing angle of attack to 35°, which is approximately where $C_{L_{max}}$ occurs, provides about a 25 percent increase in turn rate at M = 0.50. Increasing the turn rate allows the modified airplane to maneuver with the advantage of a shorter turn radius, as illustrated schematically in Figure 33 where the evading

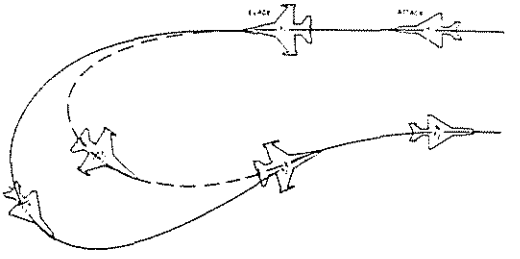

Fig. 33 - Illustration of Improved Turning Performance

aircraft is seen to turn its initial disadvantage to an advantage with a SNF turn.

These same general maneuvering results have also been presented and discussed in a more quantitative manner by Dr. W.B. Herbst of M.B.B. in Reference 10.

HIGH DECELERATION - Calculated tangential decelerating load factors are presented in Figure 34. The values of deceleration at a

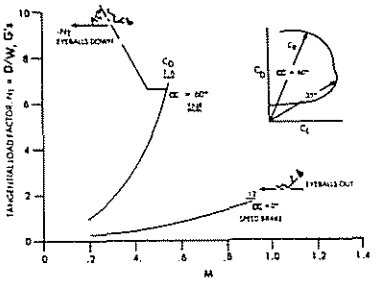

Fig. 34 - Calculated Tangential Decelerating Load Factor vs. Mach Number SNF. Z = 10k ft.

SNF angle of attack of 60° are compared with data estimated for the same aircraft equipped with speed brakes. As shown the drag coefficient

and decelerations for SNF are an order of magnitude greater than with speed brakes.

Another, more subtle, point can be drawn from these data which indicates the manner in which the deceleration vector would apply with respect to the pilots spine. SNF in this application applies the force aligned almost with the pilot's spine, "eyeballs down", a situation more natural to the pilot under maneuvering flight. On the other hand, even if the speed brake effectiveness could be improved up to the level of SNF, which is highly unlikely, the inertia forces on the pilot would cause him to "hang in the belts - eyeballs out". The "eyeballs out" direction would most probably be the least comfortable for a pilot under decelerating conditions, particularly if the loads have any appreciable vibratory components.

To summarize, very high deceleration forces can be commanded using SNF with control system modifications to allow for controlling to very high angles of attack. This use of SNF could be applied to cause an attacker to overshoot, as depicted in the decelerating position exchange illustration presented in Figure 35. Once the overshoot

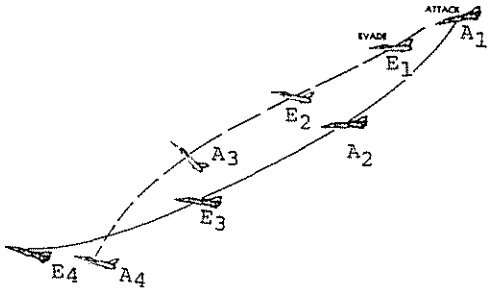

Fig. 35 - Illustration of Decelerating Position Exchange using SNF

is forced and completed the SNF-LWF pilot can convert the situation to his advantage by simply pushing over to a lower angle of attack and accelerating as or firing as required.

This maneuver, while not identical, accomplishes the same effect as Vectoring-In-Forward-Flight or "Viffing" maneuvers recently used by the British AV-8 Harrier pilots against the Argentine Mirages in the battle for the Falkland Islands.

AIMING AND POINTING - At very low speeds and high angles of attack, as shown in Figure 26, there is a potential for improving the aiming and pointing capability, in a manner similar to that of circling boxers or a slowly turning helicopter, in order to allow expansions of the LWF firing envelope.

As the angle of attack is increased further in SNF, the aircraft loses speed and the dynamic pressure decreases the stabilizing moments about the center of gravity in the same proportion in which the dynamic pressure decreases the moments generated by the aerodynamic controls. As the speed continues to decrease, the aircraft will feel more sluggish in its response to control input, until at some low speed, it will be judged to be unresponsive by the pilot. Use of reaction controls or vectored thrust, however, can alleviate this problem. Puffer controls, such as are used on the AV-8 VTOL aircraft, could be employed to change attitude in the low speed region. This advantage could be used to put the missiles carried by the LWF within a design firing envelope, thus allowing kills from very low speeds.

CONCERNS AND ADDITIONAL DATA NEEDS

Although the results of free-flight, wind tunnel, and limited analytic investigations have indicated attractive potential advantages for several aircraft classes when flown in supernormal flight, there are a number of remaining concerns, and data is required to provide the necessary confidence prior to proceeding with full-scale application and demonstration. Some of these concerns and needs are:

(1) Dynamic stability and damping coefficients cannot be calculated at angles of attack beyond the stall, and wind tunnel measurements are required.

(2) Full, six-degree-of-freedom motion studies are required to investigate potential handling quality problems associated with disturbances and cross-coupling effects.

(3) Computer and piloted simulator studies are needed to validate analytic motion study results and to develop tactical maneuvers in multi-aircraft engagements.

(4) Wind tunnel investigations are required to develop acceptable high angle of attack turbo-jet inlet performance.

(5) Dynamic model studies should be made to allow vibratory loads assessments.

(6) Aircraft design and systems studies should be made to determine the feasibility and benefits of combining advanced technologies such as active reaction controls, supercritical aerodynamics, close-coupled wing-canard configurations vectored thrust, and all-moving stabilizing and control surfaces.

(7) Methods are required for mechanizing (mechanical, electrical, or hydraulic) the all-moving tail, or large-chord elevons, in a simple, reliable, cost-effective manner.

(8) Wind tunnel and free-flight model investigations are needed to develop improved effectiveness of aerodynamic controls.

(9) Only a limited range of wing planform and control system combinations have been investigated.

SUMMARY AND RECOMMENDATIONS

Free-flight, wind tunnel, and analytic investigations of example general aviation, RPVs, and assumed modified lightweight fighter aircraft indicate the possibilities, applications, and advantages of flight at supernormal attitudes.

Supernormal flight was defined to mean safe and useful flight at attitudes such that the angles of attack (ranging from 30° to 90°) are much greater than those normally associated with maximum lift; the ranges of unaccelerated trim and control of pitch and flight path angles and those of flight path and vertical velocities, are greatly expanded; and the dynamic and accelerated maneuvering turn rates, agility, aiming, and pointing capabilities are greatly enhanced.

The essence of the primary SNF longitudinal control concept is to deflect the tail, or large chord elevons, to magnitudes of approximately the same order, but of opposite direction, as the airplane angle of attack. Although the wing is either partially or completely stalled, the effective tail aerodynamic angle of attack is less than stall and the tail is capable of providing both stability and control. At low speeds, where aerodynamic stability and control are diminished, the use of auxilliary reaction controls and/or thrust vectoring was assumed to be required and feasible to employ.

Potential applications proposed, and partially demonstrated, for a limited number of aircraft classes include:

- Stall survivability enhancement.
- Spin prevention and recovery.
- Recovery of RPVs.
- Fuel reduction on VTOL aircraft descents.
- Steep approaches to short-field landings.
- Increased instantaneous turn rates.
- High deceleration for tactical position exchange.
- Improved aiming and pointing.

It is assessed that concerns remain, and additional data are required to provide necessary confidence for full-scale applications. To allay the concerns and fill the data needs, it is recommended that:

(1) Measurements of dynamic stability and damping coefficient characteristics at very high angles of attack be conducted.

(2) Full, six-degree-of-freedom motion studies be made to investigate potential handling qualities problems associated with disturbances and cross-coupling effects.

(3) Computer and piloted simulator studies be made to validate analytic motion study results and to develop tactical maneuvers in multi-aircraft engagements.

(4) Wind tunnel investigations be undertaken to develop acceptable high angle of attack inlet performance for turbo-jet aircraft.

(5) Dynamic model studies be made for vibratory loads assessment.

(6) Aircraft design and systems studies be undertaken to determine SNF feasibility and benefits of combining advanced technologies such as active reaction controls, supercritical aerodynamics, close coupled wing-canard configurations vectored thrust, and all-moving stabilizing and control surfaces.

(7) Studies be made to develop methods for mechanizing the all-moving tail, or large-chord elevons, in a simple, reliable, cost effective manner.

(8) Wind tunnel and free-flight model investigations be made to develop improved effectiveness of aerodynamic controls.

(9) The range of wing planform control system combinations be expanded in additional wind tunnel tests.

REFERENCES

1. Chambers, Joseph R.; and Grafton, Sue B.: Aerodynamic Characteristics of Airplanes at High Angles of Attack. NASA Technical Memorandum 74097. December 1977.
2. Roberts, Lawrence T.; and Strom, Thomas H.: All-Axis Control of Aircraft in Ultra Deep Stall. Assignee: Dynamic Engineering Incorporated, Newport News, VA United States Patent 4,261,533. April 14, 1981.
3. Roberts, Lawrence T.; and Strom, Thomas H.: All-Axis Control of Aircraft in Deep Stall. United States Patent 4,099,687. July 11, 1978.
4. Goldberg, Carl: "Bring Them Down Safely". Model Airplane News, September 1943.
5. Kasper, Wietold A.: Aircraft. United States Patent 3,438,597. April 15, 1969.
6. Kasper, Wietold A.: Aircraft with Vortex Generation. United States Patent 3,831,855. August 27, 1974.
7. Kruppa, Edwards: A Wind Tunnel Investigation of the Kasper Vortex Concept. AIAA Paper 77-310. 1977.
8. Rossow, V.J.: Lift Enhancement by an Externally Trapped Vortex. AIAA Paper 76-672. 1977.
9. Bowman, James S., Jr.: Spin Tunnel Tests to Evaluate Large Horizontal Tail Deflections for Spin Recovery. NASA Spin Tunnel Movie. 1981.
10. Herbst, W.B.: Future Fighter Technologies. Journal of Aircraft. Volume 17, No. 8, August 1980. Article 80-4077.
11. Strom, Thomas H. "Dynamic Engineering Presents Flight at Supernormal Attitudes". A movie presenting selected radio controlled free-flight model results. 8 mm and 16 mm films are available for viewing at DEI facilities.
12. Bowman, James S., Jr.: Summary of Spin

Technology as Related to Light General Aviation Airplanes. NASA TN D-6575. December 1971.

13. Bryant, Robert L.: Longitudinal Trim and Tumble Characteristics of a 0.057 Scale Model of the Chance Vought XF7U-1 Airplane. NACA RM No. SL8F14.
14. Strom, Thomas H.; Paulson, John W.; and Alford, William J., Jr.: Low-Speed Wind Tunnel Investigation of the Aerodynamic Characteristics of a 0.25 Scale Model Similar to a Low Wing Two-Place General Aviation Aircraft at Supernormal Angles of Attack. DEI Document No. D-051 (DP-8157-04). 1982.
15. Chambers, Joseph R.: Overview of Stall/Spin Technology. AIAA Paper 80-1850, 1980.
16. Bihrle Associates: Static Aerodynamic Characteristics of a Typical Single-Engine Low-Wing General Aviation Design for an Angle of Attack Range of -8° to 90°. NASA CR-2971, July 1978.
17. Knight, Montgomery: Wind Tunnel Tests on Autorotation and the "Flat Spin". NACA Report No. 273.1927.
18. Alford, William J., Jr.: Potential Trimmed Flight Path Characteristics of a Modified Light Weight Fighter Airplane at Supernormal Angles of Attack. Dynamic Engineering Technical Report TR-059. March 29, 1982.
19. Gainer, Thomas G.; and Hoffman, Sherwood: Summary of Transformation Equations and Equations of Motion used in Free-Flight and Wind-Tunnel Data Reduction and Analysis. NASA SP-3070. 1972.
20. Blanchard, W.S., Jr.: A Flight Investigation of the Ultra-Deep-Stall Descent and Spin Recovery Characteristics of a 1/6 Scale Radio-Controlled Model of the Piper PA-38 Tomahawk. NASA Contractor Report 156871, March 1981.
21. Taylor, Robert T.: Enhanced Agility in Light Weight Combat Aircraft Through the use of Supernormal Flight. Dynamic Engineering Document No. D-060. May 15, 1982.
22. Nguyen, Luat T.; Ogburn, Marilyn E.; Gilbert, William P.; Kibler, Kemper S.; Brown, Phillip W.; and Deal, Perry L.: Simulator Study of Stall/Post-Stall Characteristics of a Fighter Airplane with Relaxed Longitudinal Static Stability. NASA Technical Paper 1538. December 1979.
23. Salvatori, V.L. from Briefing Entitled, "Supernormal Flight Applications". 1982.

APPENDIX A - SYMBOLS & NOMENCLATURE

The definitions of flight path and force nomenclature are presented in Figure 1.

C_R	Resultant force coefficient, $\frac{R}{qs} = \sqrt{C_L^2 + C_D^2}$
C_L	Lift coefficient, $\frac{L}{qs}$
C_D	Drag coefficient, $\frac{D}{qs}$
C_m	Pitching moment coefficient, $\frac{m}{qsc}$
L	Lift
D	Drag
L/D	Lift-to-drag ratio
m	Pitching-moment
p	Rolling velocity
q	Dynamic pressure, $\frac{1}{2}\rho V^2$
S	Wing reference area
ρ	Air density
T	Thrust
W	Airplane weight
X,Y	Flat earth coordinate system
V	Flight path velocity
$\dot{z}$	Vertical velocity
α	Angle of attack
γ	Flight path angle
θ	Pitch angle
δ_h	Stabilator deflection
Λ	Sweep angle
ε	Downwash angle
$\dot{X}$	Horizontal velocity, dx/dt
$\frac{\partial C_R}{\partial \alpha}$	Slope of resultant force coefficient vs. α
C_ℓ	Rolling-moment coefficient, referred to the aircraft X or longitudinal axis, $\frac{\ell}{qSb}$
C_n	Yawing-moment coefficient, $\frac{n}{qSb}$
C_{ℓ_β}	Effective dihedral parameter
ΔC_{ℓ_a}	Incremental rolling moment due to aileron deflection
ΔC_{ℓ_r}	Incremental rolling moment due to rudder deflection
$C_{m_{\delta_h}}$	Horizontal tail control parameter
C_{n_β}	Directional stability parameter
ΔC_{n_a}	Yawing-moment due to aileron deflection
ΔC_{n_r}	Rudder control effectiveness parameter
α_t	Horizontal tail angle of attack
C_{ℓ_p}	Damping in roll parameter